CHAPTER IV
RESULTS AND DISCUSSION

4.1 Characterization of MCM-48 and Pd-MCM-48

The synthesized MCM-48 and Pd-MCM-48were characterized using low-angle XRD, as shown in Fig. 4.1 and 4.2. Figure 4.1shows the XRD pattern of pure MCM-48, indicating four well-resolved diffraction peaks in the 2θ range of 2–6°, indexing to the diffraction of {211}, {220}, {420}, and {322}. These peaks are the characteristics of the cubic ordered structure of MCM-48. (Longloilert *et al.*, 2011)

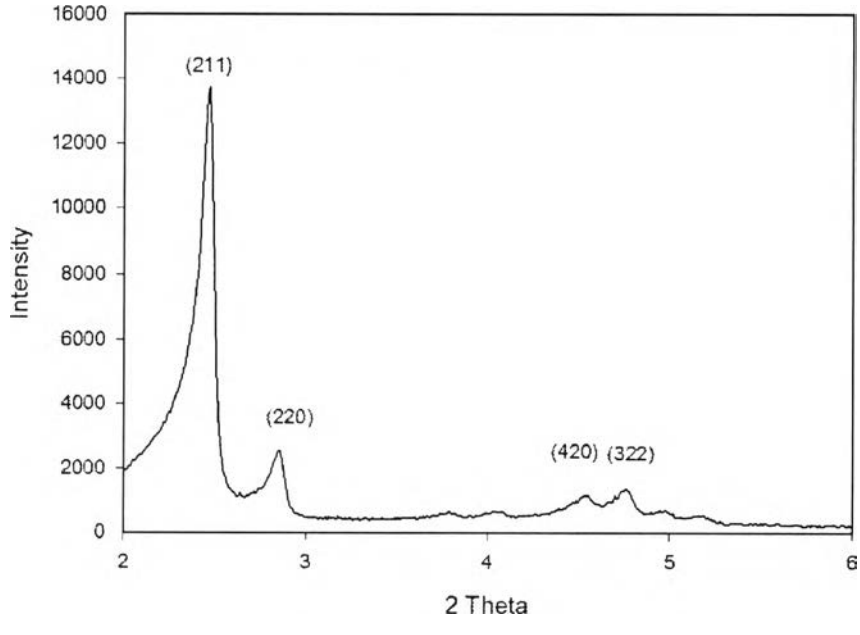

Figure 4.1 XRD pattern of pure MCM-48.

The XRD patterns in Fig. 4.2 of various Pd-MCM-48 containing different amounts of Pd (1–5%) synthesized by impregnation method show all diffraction peaks matched well with the patterns of the pure MCM-48. Therefore, the ordered mesoporous MCM-48 structure was not collapsed after the introduction of palladium species. However, when Pd was loaded onto MCM-48, the d_{211} and d_{220} peaks shifted to a higher angle. This finding is consistent with the previous work reported by Yin

et al, in 2011. Pd may have been embedded into the MCM-48 channel, causing the *d*-spacings of the {211} and {220} planes to decrease, resulting in a shift of the d_{211} and d_{220} peaks to a higher angle.

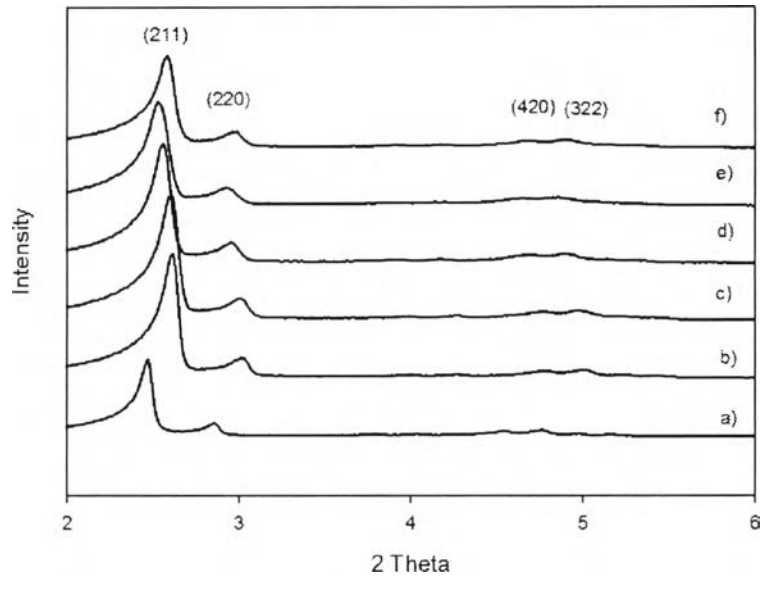

Figure 4.2 XRD patterns of a) MCM-48, b) 1, c) 2, d)3, e) 4, and f) 5%Pd-MCM-48.

To observe the Pd species in Pd-MCM-48, wide-angle XRD was performed, see Fig. 4.3. It was found a very broad band centered about 23°, attributed to SiO_2. The Pd species was found in the form of PdO at $2\theta = 34°$, corresponding to {101} PdO. The intensity of {101} PdO diffraction peak increases with increasing Pd content, resulting from more Pd metal loaded. The other relative peaks of PdO were also observed at $2\theta = 43°$ and 55°, indexing to {110} and {112} plane, respectively. (Teranishi *et al.*, 1998, Yin *et al.*, 2008, Abate *et al.*, 2011 and Duan *et al.*,2012). It is worth noting that the peak of Pd^0 was not observed.

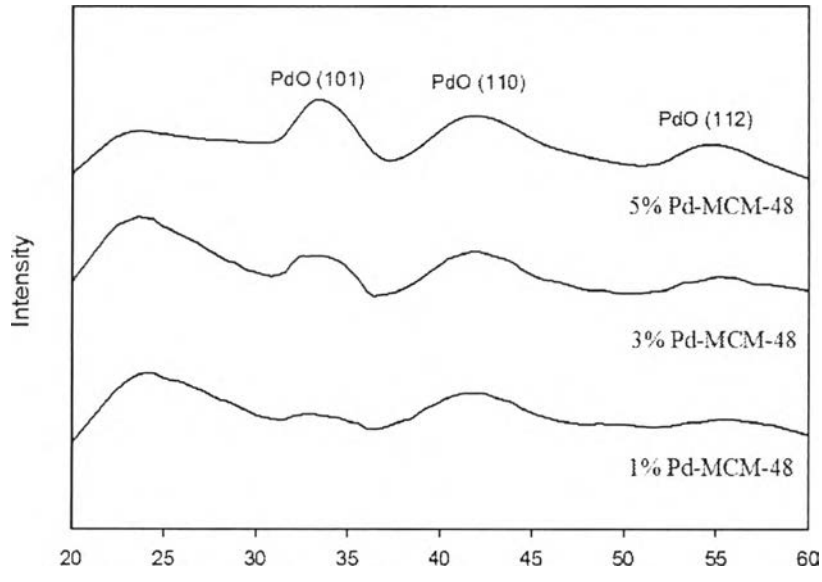

Figure 4.3 Wide-angle XRD patterns of a) 1, b) 3, and c) 5%Pd-MCM-48.

The synthesized catalysts were characterized N_2-adsorption and desorption isotherms, as illustrated in Fig. 4.4. Those obtained isotherms were similar to the isotherms of type IV, according to IUPAC classification, corresponding to the typical characteristics of mesoporous materials. At the relative pressure P/P_0 between 0.2 and 0.4, the isotherms exhibit a sharp inflection characteristic of capillary condensation with regular mesopores. (Yang *et al.*, 2005, Longloilert *et al.*, 2011, Kalbasi *et al.*, 2012)

BET specific surface areas, pore volumes as well as pore diameters of MCM-48 and Pd-MCM-48 were calculated using BET and BJH method (Table 4.1). The pore size distribution curves resulted in very narrow peaks centered at about 2.1–2.4 nm. This is attributed to the mesopore ordering with well-defined pore structures, the data obtained coincide well with those already reported by Ajaikumar *et al.* (2008). It is seen that the synthesized catalysts has a high BET surface area in a range of 1530–1620 m^2/g and a pore volume of around 0.9 cc/g. Expectedly, as the Pd loading increased, the surface area and the pore volume decreased owing to some blockage of Pd in the pores.

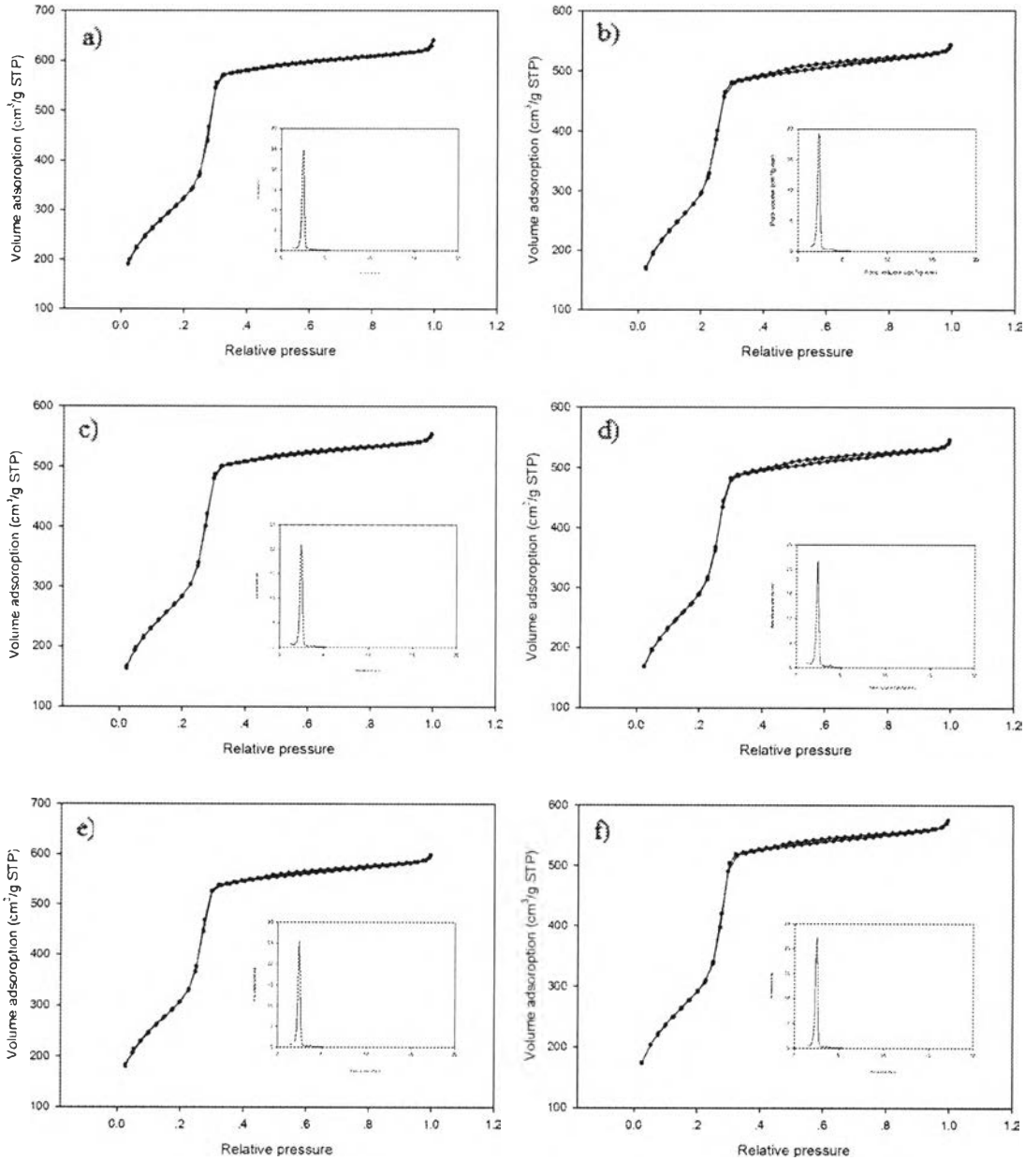

Figure 4.4 N_2-adsorption and desorption isotherms of a) Pure MCM-48, b) 1, c) 2, d) 3, e) 4, and f) 5%Pd-MCM-48.

Table 4.1 Pore structure parameters of MCM-48 and Pd-MCM-48

Sample	surface area (m^2/g)	pore size (nm)	pore volume (cc/g)
Pure MCM-48	1593	2.445	0.9736
1%Pd-MCM-48	1535	2.167	0.8317
2%Pd-MCM-48	1481	2.257	0.8357
3%Pd-MCM-48	1579	2.326	0.9181
4%Pd-MCM-48	1436	2.254	0.8497
5%Pd-MCM-48	1401	2.431	0.7893

Figure 4.5 shows the SEM images of pure MCM-48 and Pd-MCM-48. As can be seen, there is no significant difference between pure MCM-48 and all Pd-MCM-48 samples. All samples exhibit the truncated octahedral shape of aggregated MCM-48 particles. (Longloilert *et al.*, 2011) Therefore, loading Pd on MCM-48 retained the morphology and cubic-type ordering structure of pure MCM-48. This statement was assured using the previous XRD results.

The TEM images, Fig.4.6, show the pore structure along cubic {100} direction with a uniform channel system, as reported by Longloilert *et al.* (2011). Figure 4.6a is the TEM image of 1%Pd-MCM-48, indicating that no obvious extra phases of the Pd species are present outside of the mesoporous structure. For Fig. 4.6b, 5%Pd-MCM-48, the dark spots were observed, corresponding to Pd particles agglomerate on the external surface. (Kalbasi *et al.*, 2012)

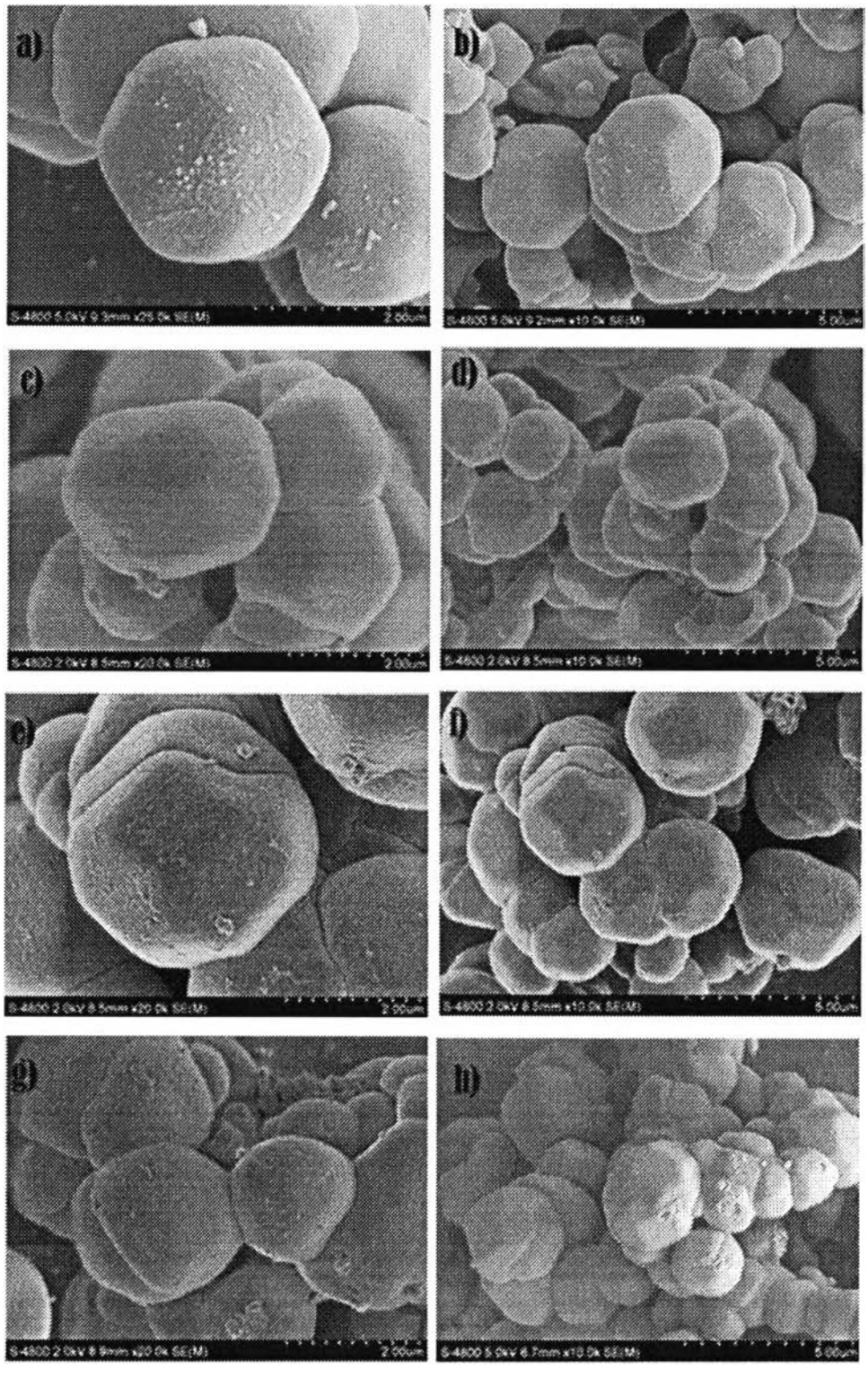
a)
b)
c)
d)
e)
f)
g)
h)

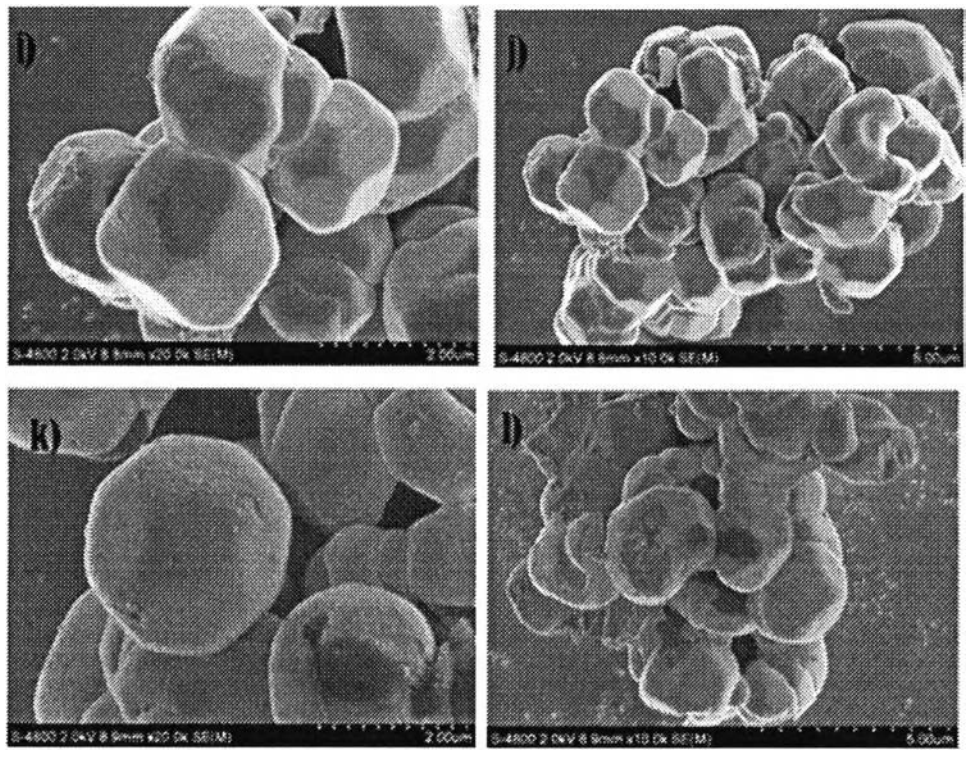

Figure 4.5 SEM images of a,b) MCM-48, c,d) 1, e,f) 2, g,h)3, i,j) 4, and k,l) 5%Pd/MCM-48 (magnifications of a, c, e, g, i, k and b, d, f, h, j, l are ×20k and ×10k, respectively).

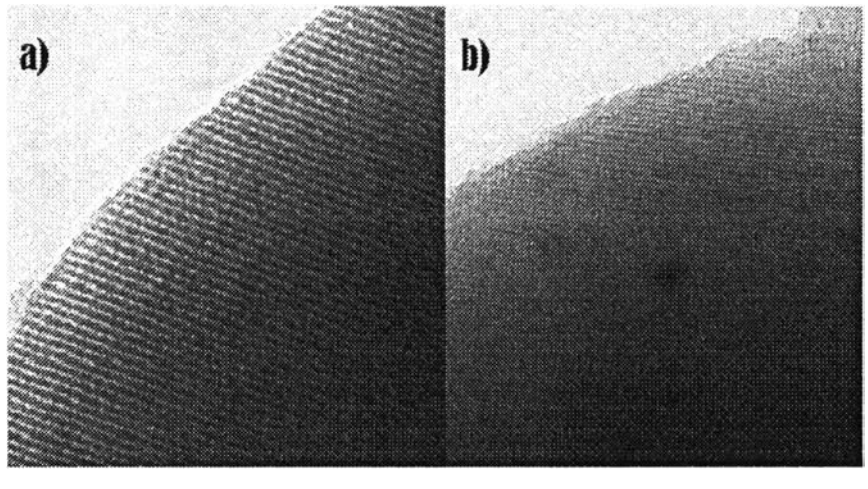

Figure 4.6 TEM images of Pd-MCM-48; a) 1 and b) 5%Pd-MCM-48.

The Pd contents in the synthesized products were analyzed by XRF and summarized in Table 4.2. The results clearly confirm the presence of palladium in the catalyst although the obtained contents were much less than the actual adding.

These results may be owing to poor dispersion or agglomeration of the Pd species in the support, giving the fact that main part of the catalyst contained mostly only MCM-48.

Table 4.2 XRF analysis of Pd-MCM-48

Sample	Si (%)	O (%)	Pd (%)
1%Pd-MCM-48	38.759	61.233	0.008
2%Pd-MCM-48	33.005	66.983	0.012
3%Pd-MCM-48	39.873	60.104	0.023
4%Pd-MCM-48	37.819	62.155	0.026
5%Pd-MCM-48	36.785	63.187	0.028

The type of Pd species created inside the pores and channels of the support was revealed by UV reflectance spectra (DR-UV) (Fig. 4.7). They are associated with the presence of PdO. The curves showed two wide bands peaking at 395, and 520 nm. The first band is attributed to a d-d transition and the other at 520 nm to a bulk PdO. The four bands were more outstanding if Pd content was added, indicating that larger Pd species were present. (Cheikhi *et al.*, 2005, Cónsul *et al.*, 2006)

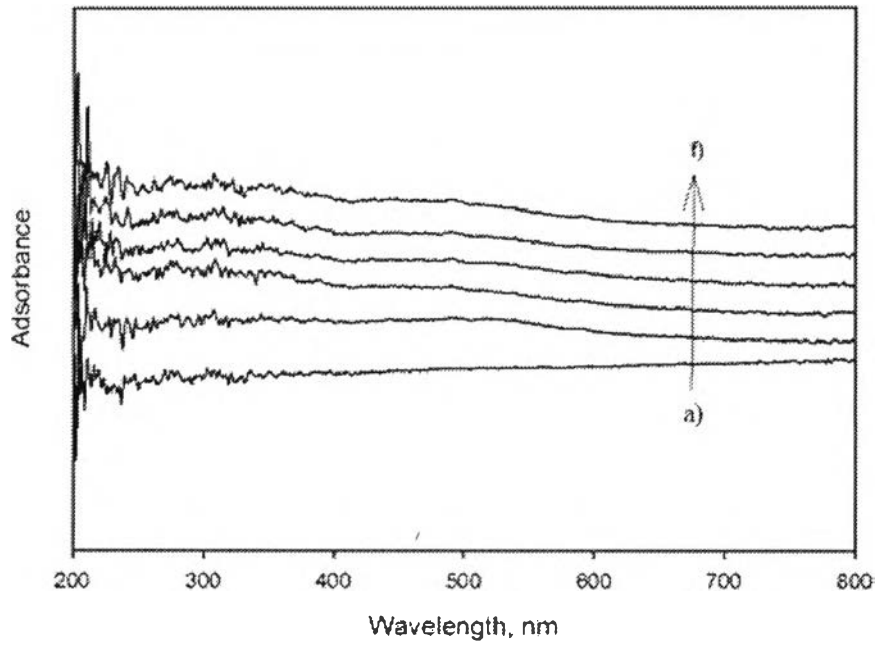

Figure 4.7 UV-Vis spectra of a) MCM-48, b) 1, c) 2, d) 3, e) 4, and f) 5%Pd-MCM-48.

Temperature programmed reduction (TPR) profiles of Pd-MCM-48 catalysts are demonstrated in Fig. 4.8. In general, hydrogen consumption is observed at room temperature due to PdO reduction to form PdH_x species, and upon temperature generation of H_2 occurs to give a negative signal during TPR analysis at around 100 °C, as clearly observed from 3 and 5% Pd-MCM-48. This result was consistent with those reported by Cubeiro *et al.* (1988), Cheikhi *et al.*(2005), and Ivashchenko *et al.*(2012).

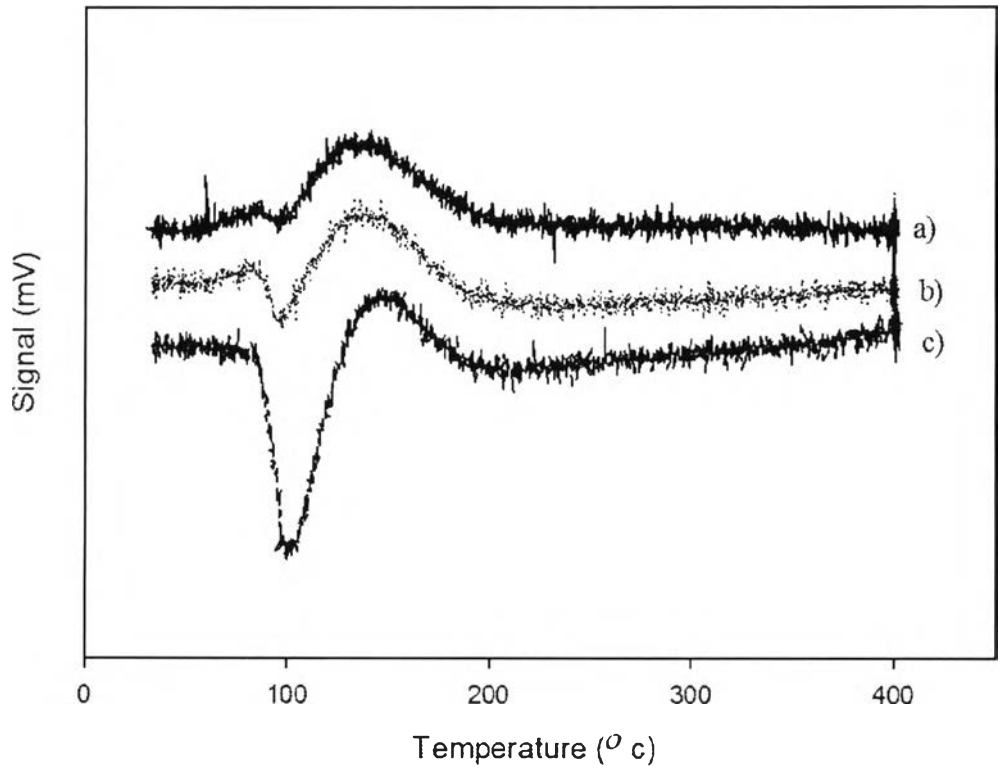

Figure 4.8 TPR profiles of a) 1, b) 3, and c) 5%Pd-MCM-48.

Both Cubeiro *et al.* (1988) and Ivashchenko *et al.* (2012) also reported that when increasing temperature to higher, the complete reduction of palladium oxide species took place, giving a positive peak around 150 °C, suggesting that palladium species were responsible for such a peak from strong interaction with the carrier or support. Their observation was also noticeable in our case such that hydrogen participates in the reduction reaction of palladium oxide species, as shown in Eq.1

$$H_2 + PdO \longrightarrow Pd + H_2O \qquad (1)$$

The ratios of the integral area under the curve between the negative and the positive peaks of 3 and 5%Pd-MCM-48 were 0.11 and 4.61, respectively. It can be suggested that the higher palladium content led to the easier PdH_x formation at room temperature during TPR analysis.

4.2 Activity study

Suzuki–Miyaura cross-coupling reaction (Fig. 4.9) involves the reaction of phenylboronic acid and aryl halide in the presence of palladium catalyst and base in solvent via microwave hydrothermal treatment.

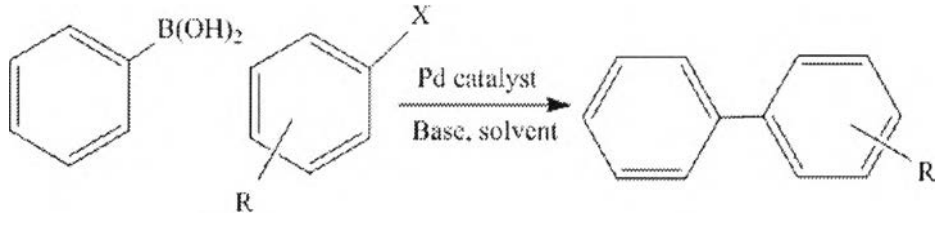

Figure 4.9 Suzuki–Miyaura cross-coupling reaction.

For several researches, palladium-catalyzed Suzuki reaction generally needed Pd^0 containing organometallic compounds, such as $Pd(Phh_3)_4$, $[Pd_2(dba)_2]$ (dba= dibenzylideneacetone), $[Pd(OAc)_2]$, etc., which are not only air/moisture sensitive, but also tend to form clusters. Consequently, the more readily accessible precatalysts were utilized (Mitchell, 2008).In this work, Pd-MCM-48 was chosen to replace those Pd^0 containing organometallic compounds because of its air stability, ease to prepare, store, and use, no need to use in a glove box.

The catalytic activity of the synthesized Pd-MCM-48 on microwave-assisted Suzuki reaction is given in Table 4.3. The microwave-assisted reaction of phenylboronic acid with 1-bromo-4-fluorobenzene was conducted by using various Pd contents loaded on MCM-48 (1, 3, and 5%) and K_2CO_3 as a base in DMF solvent. The results evidently indicated that the optimal reaction time was 20 min at 120 °C, giving the highest conversion (42.3%) of 4-fluoro-1,1'-biphenyl and 3-fluoro-bromobenzene when 5%Pd-MCM-48 was used as the catalyst.

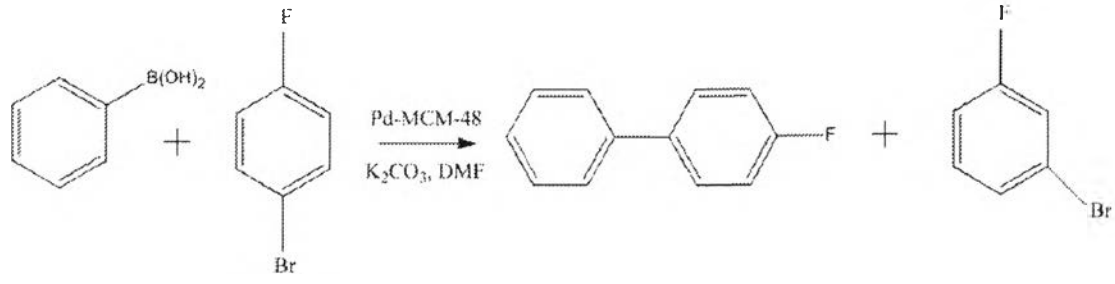

Figure 4.10 Suzuki–Miyaura cross-coupling reaction in this study.

At the same reaction conditions as 5%Pd-MCM-48, 3%Pd-MCM-48 provided slightly less conversion of 39.4% than 5%Pd-MCM-48, indicating that the Pd content in the catalyst may affect the reaction conversion. This assumption can be confirmed from the results obtained from using pure MCM-48 and 1%Pd-MCM-48. No reaction was taken place although the reaction was kept for 30 min. Considering the XRF results in Table 4.2, the analyzed Pd in 1%Pd-MCM-48 was very low and this could be another reason why the reaction did not take place. For 3%Pd-MCM-48, when the reaction was conducted for 10 min, no product was observed, indicating that the reaction time was too short. However, if the Pd content was increased to 5%, very small amount of the conversion (1.9%) would be generated after 10 min reaction time. Interestingly, when the reaction time was increased to 30 min, the product was decreased for both 3 and 5%Pd-MCM-48. The reason could be that loss of catalytic surface area, support area, and active phase–support reactions could occur after too long reaction time. (Bartholomew, 2001)

Table 4.3 Microwave-assisted Suzuki reaction using various Pd-MCM-48 catalysts at 120 °C for different reaction times

Catalyst	Time (min)	% Conversion	% Selectivity	
			Major product	By product
MCM-48	10	-	-	-
	20	-	-	-
	30	-	-	-
1%Pd-MCM-48	10	-	-	-
	20	-	-	-
	30	-	-	-
3%Pd-MCM-48	10	-	-	-
	20	39.4 ± 2.9	97.2	3.0
	30	17.0 ± 0.8	91.1	8.9
5%Pd-MCM-48	10	1.9 ± 1.6	100	-
	20	42.3 ± 4.9	93.1	6.9
	30	27.0 ± 1.7	98.1	1.9

Generally, Suzuki–Miyaura cross-coupling reaction is catalyzed by Pd^0 species, but in this study the required product was obtained although only PdO species were observed. The reason was explained by Masuyama *et al.* (2012) that the Pd^0 species easily occurred from the reduction of Pd^{2-} species by boron compound. The mechanism of the Suzuki cross-coupling reaction was reported by Lindholm in

2011, see Fig. 4.10. The cross-coupling reaction proceeded according to a catalytic cycle, involving the oxidative addition of haloarenes or other electrophiles to the palladium(0) complex, yielding Ar-Pd(II)-X, followed by transmetallation and reductive elimination steps.

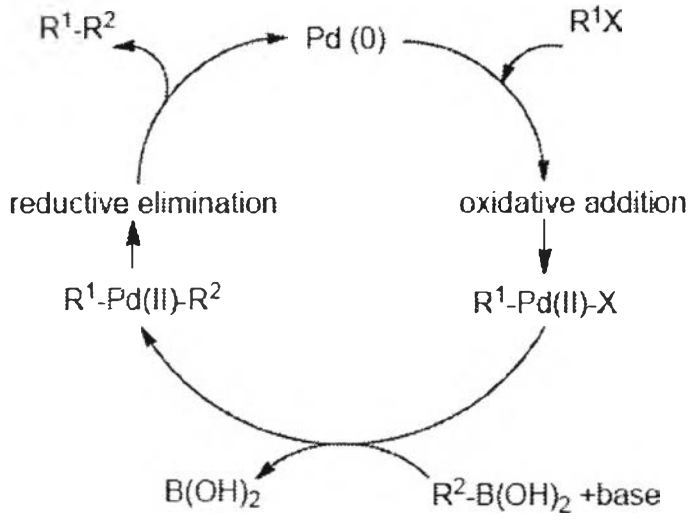

Figure 4.11 Catalytic cycle, the mechanism of the cross-coupling reaction. (Lindholm, 2011)

Therefore, the mechanism of Pd-MCM-48 catalyzed Suzuki cross-coupling reaction in this study may involve the oxidative addition of 1-bromo-4-fluorobenzene to the Pd^0 reduced from Pd^{2+} to form the organopalladium halide (Ar_1–Pd(II)–Br). This reaction is followed by transmetallation between pinacol ester of diboronic acid and Ar_1-Pd(II)-Br with the aid of base to gain Ar_2-Pd(II)-$B(OR)_2$ intermediate and provide diorganopalladium complex (Ar_1–Pd(II)–Ar_2), which undergoes a reductive elimination, leading to carbon carbon bond formation and regeneration, as shown in Fig. 4.11

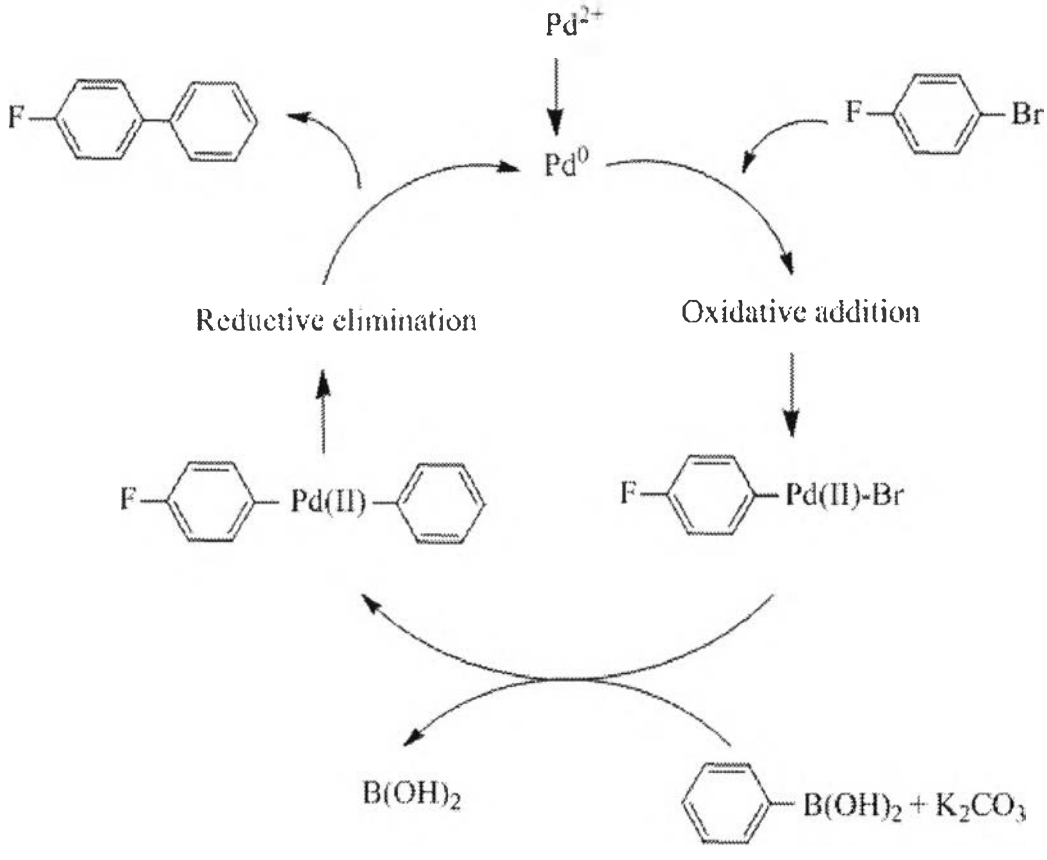

Figure 4.12 Catalytic cycle, the mechanism of the cross-coupling reaction in this study.

Alrawashdeh (2011) indicated that for palladium-catalyzed cross coupling reactions, ligand played a key role in modulation and improvement of the given catalytic capacity of the metal. The ligands in conjunction with a palladium source were attributed to a combination of both electronic properties, which facilitated the oxidative addition, and steric hindrance, which favored the reductive elimination steps in the catalytic cycle. However, in this case the Pd species in the form of PdO contained no ligand, resulting in the lower conversion (<50%).

In this work, to prove whether the Pd species type would affect the Suzuki reaction activity, PdO in 5%Pd-MCM-48 was thus reduced to Pd(0), as shown in Eq.1. It was found that the %conversion was slightly increased when the reaction was carried out for 20 min (48%). This result probably confirms that big ligands of

the Pd species in the Suzuki reaction play an important role in the reaction, as discussed previously.